JOURNAL OF PHYSICAL ORGANIC CHEMISTRY
J. Phys. Org. Chem. 2002; **15:** 148–153
DOI:10.1002/poc.470

Space-demanding intramolecular isomerizations in the solid state

G. Kaupp,[1]* J. Schmeyers,[1] M. Kato,[2] K. Tanaka[3] and F. Toda[4]

[1]Organische Chemie I, Universität Oldenburg, Postfach 2503, D-26111 Oldenburg, Germany
[2]Division of Material Science, Graduate School of Human Culture, Nara Women's University, Nara 630-8506, Japan
[3]Department of Applied Chemistry, Faculty of Engineering, Ehime University, Matsuyama, Ehime 790-8577, Japan
[4]Department of Chemistry, Faculty of Science, Okayama University of Science, Ridaicho 1-1, Okayama 700-0005, Japan

Received 21 June 2001; revised 16 October 2001; accepted 8 November 2001

epoc

ABSTRACT: The thermal isomerizations of *meso*- and *rac*-3,4-dibromo-1,6-diphenyl-1,6-bis(*p*-tolyl)-1,2,4,5-hexatetraene (**1**) to give stereospecifically the 3,4-bis(phenyl-*p*-tolylmethylene)-1,2-dibromocyclobutenes **3** and **5** + **6** were studied in the solid state using atomic force microscopy (AFM) and interpreted on the basis of known crystal structural data. These isomerizations run to completion in the bulk and include highly space-demanding internal rotations around the central bond. Far-reaching anisotropic molecular movements are detected on the major faces that align the surface features along cleavage planes in the initial phase rebuilding stage. Only one of three identified cleavage planes of *meso*-**1** is successful, owing to closer interactions of the bromine substituents in the non-used cleavage planes. Thus, very fine details can be correlated and predicted for the occurrence of internal rotations and molecular movements in the crystal lattice. The second stage in these intramolecular isomerizations, the phase transformation, produces very high features up to 100 nm and still parallel to the preferred cleavage plane of *meso*-**1** but in the μm range without relation to the initial crystal structure in the case of *rac*-**1**. Copyright © 2002 John Wiley & Sons, Ltd.
Additional material for this paper is available from the epoc website at http://www.wiley.com/epoc

KEYWORDS: atomic force microscopy; crystal packing; diallenes; molecular migrations within the crystal; thermal solid–solid isomerization

INTRODUCTION

E/Z isomerizations in the solid state have been described, modeled and mechanistically investigated in terms of rotational[1] and twist mechanisms.[2] A di-*tert*-butyltetraphenylbisallene isomerized only in the surface region and at cracks of the crystal, as there was no way to accommodate the molecular movements with the crystal packing, and the macroscopic crystal shape did not change.[3] Further highly substituted diallenes have been found to undergo space-demanding conformational changes and cyclizations in the crystalline state up to full conversion in a stereoselective manner.[4,5] The macroscopic crystal shape was retained, but the opaqueness indicated a non-topotactic (for topotactic relationships, see Ref. 6) reaction course. It was Kohlschütter who coined the term 'topochemistry' in his famous paper of 1919[7] for that type of crystal reaction [he produced colloidal Al_2O_3 from $KAl(SO_4)_2 + NaOH/H_2O$ without collapse of the original crystal shape]. We were interested in the solid-state mechanism and report our atomic force microscopy (AFM) results on the isomerization of *meso*- and *rac*-3,4-dibromo-1,6-diphenyl-1,6-di-(*p*-tolyl)-1,2,4,5-hexatetraene (**1**).

Scheme 1 depicts the chemistry involved when *meso*-**1** or *rac*-**1** is thermolyzed. Heating of *meso*-**1** in xylene or in the solid state gives only **3**, whereas heating of *rac*-**1** in xylene or in the solid state gives 1:1 mixtures of **5** and **6**.[4]

All cyclizations occur undoubtedly from intermediate helical *s-cis*-conformers (**2** and **4**) that have to be formed initially. The cyclizations are stereoselective and occur in the formally 'conrotatory' manner[4,5] without severe steric interactions. Crystal structure determinations proved the initial *s-trans* structures of *meso*-**1** and *rac*-**1**.[4]

AFM RESULTS

Single crystals of *meso*-**1** (laths) were probed on the (010) face with the AFM before and after heating at 130 °C for 1, 3, 5, 7, 10 and 15 min. The initial crystal exhibited submicro grooves parallel to the long crystal edge [Fig.

*Correspondence to: G. Kaupp, Organische Chemie I, Universität Oldenburg, Postfach 2503, D-26111 Oldenburg, Germany.
E-mail: kaupp@kaupp.chemie.uni-oldenburg.de

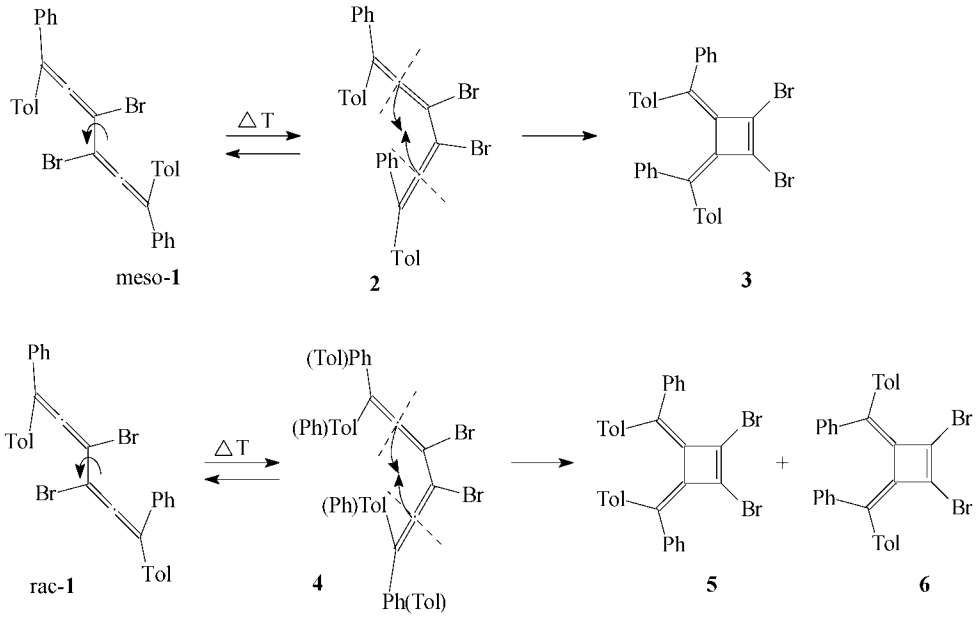

Scheme 1. Thermal transformation of *meso*-**1** and *rac*-**1** with the presumed intermediate *s-cis*-conformers and product structures

1(a)]. These became deeper upon heating [Fig. 1(b)]. Further heating produced more extended hills with grooves on them [Fig. 1(c)] and still larger wide hills in Fig. 1(d), all parallel to the long crystal edge. The conversion in Fig. 1(d) was judged to be 91% in parallel experiments (see Experimental). Clearly, we observe the

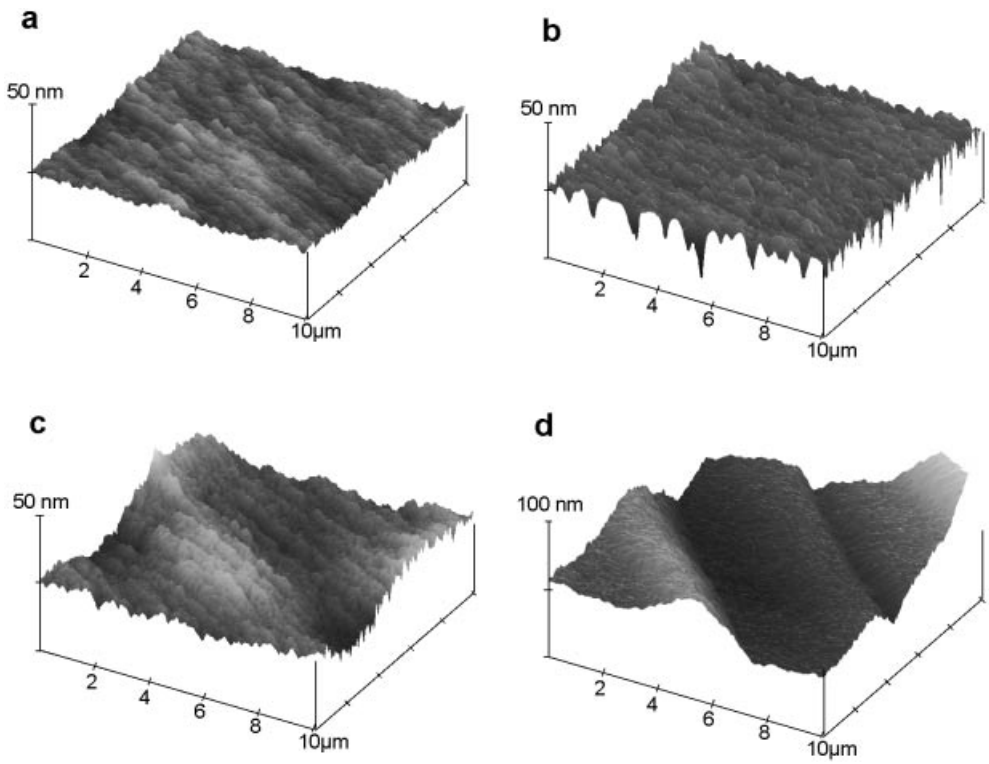

Figure 1. AFM images of *meso*-**1** (*P*-1) on (010) after heating at 130 °C: (a) 0 min, max. height 8.28 nm; (b) 5 min, max. height 33.59 nm; (c) 10 min, max. height 24.30 nm; (d) 15 min, max. height 95.19 nm. The crystal was measured at slightly varying orientations for the best results, but the features were oriented parallel to the long crystal axis in all cases. High- and low-resolution VRML images of (a)–(d) are available at the epoc website at http://www.wiley.com/epoc

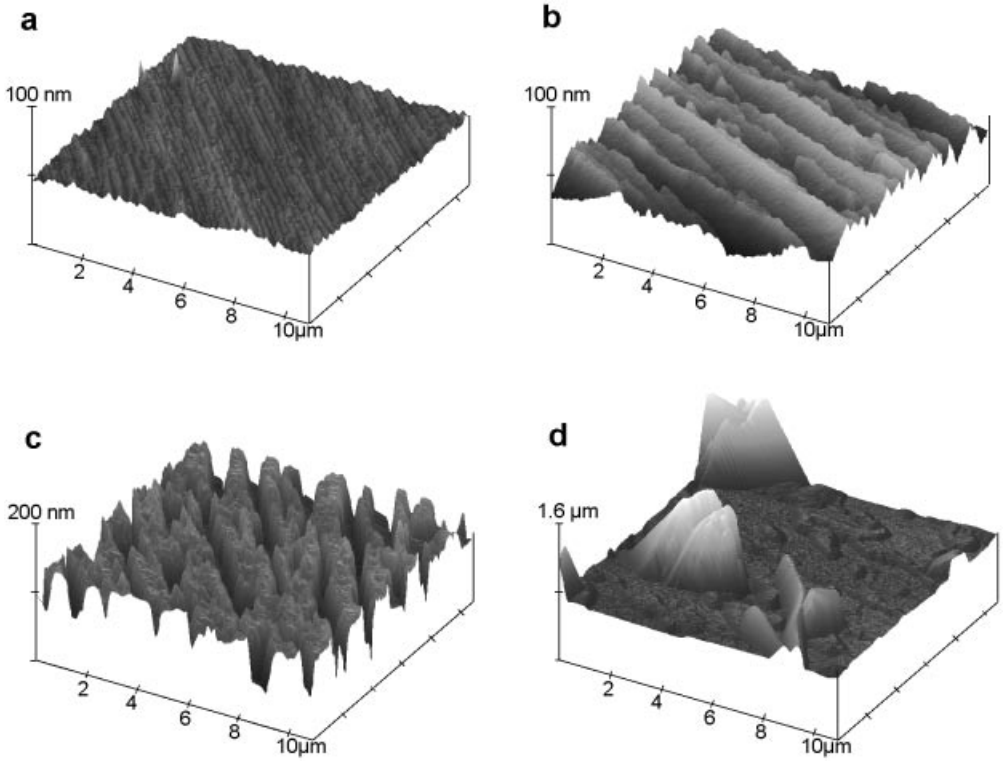

Figure 2. AFM images of *rac*-**1** ($P2_1/n$) on (–101) after heating at 130 °C: (a) 0 min, max. height 28.24 nm; (b) 15 min, max. height 37.45 nm; (c) 25 min, max. height 131.27 nm; (d) 30 min, max. height 995.35 nm. The features in (a), (b) and (c) align along the diagonal of the crystal surface; some slopes in (d) are too steep and thus suffer from tip/sample convolution. High- and low-resolution VRML images of (a)–(d) are available at the epoc website at http://www.wiley.com/epoc

occurrence of long-range molecular movements and two different stages in the solid-state reaction: phase rebuilding in the initial stage and phase transformation as soon as enough product molecules **3** have formed.[1] The high anisotropy of the feature formation indicates close relation to the crystal packing.[1,3]

A different crystal structure of *rac*-**1** (to give **5** and **6**) should lead to AFM results that are different from those with *meso*-**1** (to give **3**). Single crystals of *rac*-**1** (plates) were probed on their (–101) face before and after heating at 130 °C for 3, 6, 15, 25 and 30 min. The initial minor grooves along the diagonal [Fig. 2(a)] increased gradually after 15 min [Fig. 2(b)] and formed a heights and valleys scenery after 25 min [still diagonal, Fig. 2(c)]. Continued heating at 130 °C for another 5 min produced very large features in the µm range that no longer correlated with the original crystal packing. Figure 2(d) was taken at a site between numerous deep cracks in various directions that could no longer be traced with the cantilever contact AFM but could be seen under a light microscope at 100-fold magnification. Clearly, phase transformation to the product phase[1] occurred between these two last measurements. The conversions were judged with parallel experiments (see Experimental) to be 52% in Fig. 2(b) and 96% in Fig. 2(d). These experiments and the previous preparative results[4,5] clearly indicate that we have bulk reaction and not just changes at the surface. The red color that is additionally observed[4,5] (persistent shoulder in $CHCl_3$ at 456 nm obeying Beer's law) derives from as yet undetermined side-products (5%), but that feature does not interfere with the conclusions for the high-yield reactions.

CRYSTALLOGRAPHIC INTERPRETATION

The crystals of *meso*-**1**[4] exhibit three cleavage planes, (1–10), (–111) and (–101), that cut the (010) plane at 65°, 61° and 83° [Fig. 3(a) and (b)]. The first runs along c in the $[a + b]$ direction, the second along the $[a + b]$ and $[a + c]$ directions and the third along b in the $[a + c]$ direction. The cleavages can be executed by touching the (010) face of plates of *meso*-**1** with a needle.

Interestingly, the AFM features that are expected to align along cleavage planes (because molecules move easier there) choose only the direction of c. Therefore, apparently, the internal rotations and/or the molecular migrations are easier in the (1–10) cleavage plane. The cleavage planes (–111) and (–101) are not used for the internal rotations and/or molecular migrations because they exhibit short Br—Br distances of 3.940 Å. These seem to impede both events. Conversely, the Br—Br distance x is 6.226 Å in the (1–10) cleavage plane (the

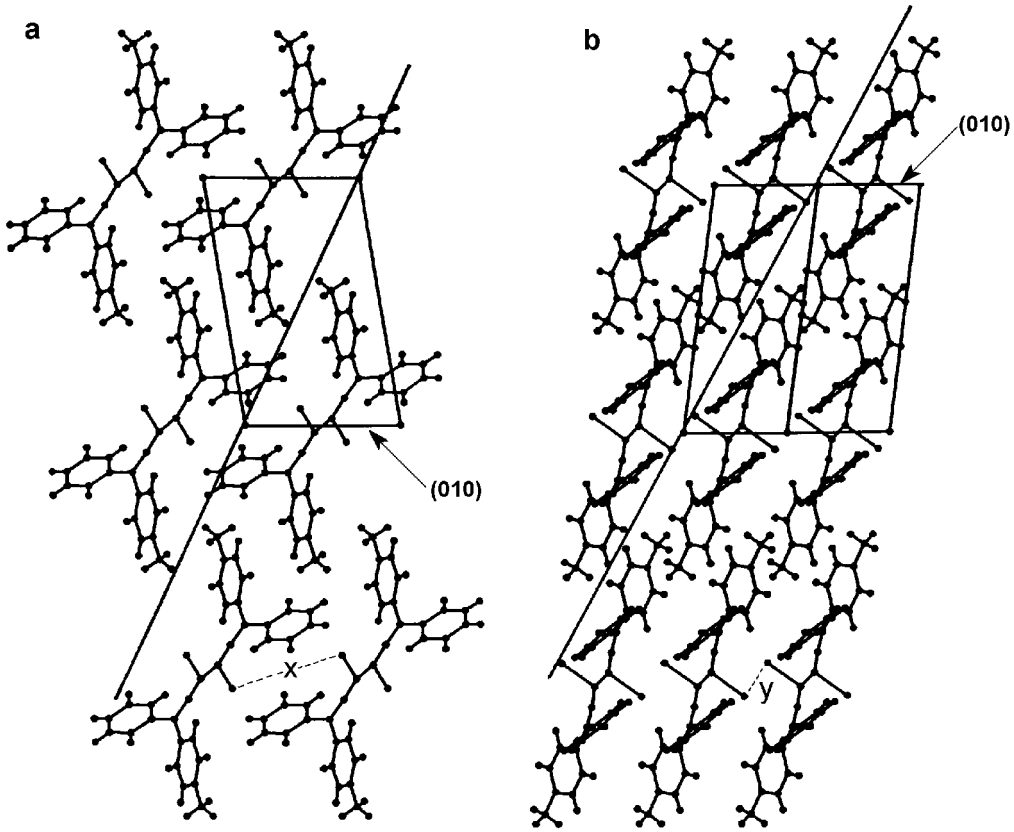

Figure 3. Molecular packing of *meso*-**1**: (a) along [001] showing the direction of the skew (1–10) cleavage plane ($x = 6.226$ Å); (b) along [101] showing the direction of the skew (–111) cleavage plane ($y = 3.940$ Å); the (–101) cleavage plane parallel to *b* is better seen in Fig. 4

staple distance to the next molecules is 6.049 Å). These facts predict the choice of only that cleavage plane for the feature formation. The strict correlation of the molecular movements with the crystal structure is clearly demonstrated by the alignment of the features along the [001] direction in Fig. 1.

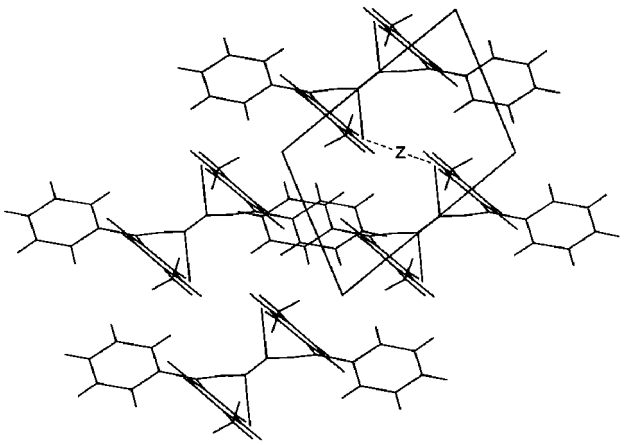

Figure 4. Molecular packing of *meso*-**1** along [010] showing the horizontal (–101) cleavage plane (parallel to the *b*-axis), that is not easily seen in Fig. 3(b), cutting the (010) surface diagonally ($z = 3.940$ Å)

The AFM features found on the (–101) face of *rac*-**1**[4] are also correlated with the crystal packing. No cleavage planes can be identified. However, the molecules align along the diagonal of the crystal on (–101) between the natural side faces (011) and (01–1) in the vertical direction of Fig. 5. It can be judged that the molecules find empty space for the required internal rotation and cyclization and that their interlocking will thereby decrease so that molecular movements above (–101) along the diagonal of the crystal will occur as observed in the phase rebuilding stage.

DISCUSSION

The thermal unimolecular solid-state reactions of **1** exhibit the same two-step molecular movements, first in the phase rebuilding and second in the phase transformation, as in gas–solid, solid–solid and non-topotactic solid-state photochemical reactions.[1] Both stages are clearly distinguishable at the surface with AFM. A peculiarity is the absence of a macroscopic crystal disintegration, that seems not to be required here, while microscopic cracks can be observed under a light microscope at 100-fold magnification. The phase rebuilding is strictly related to the crystal packing as cleavage planes and void spaces are

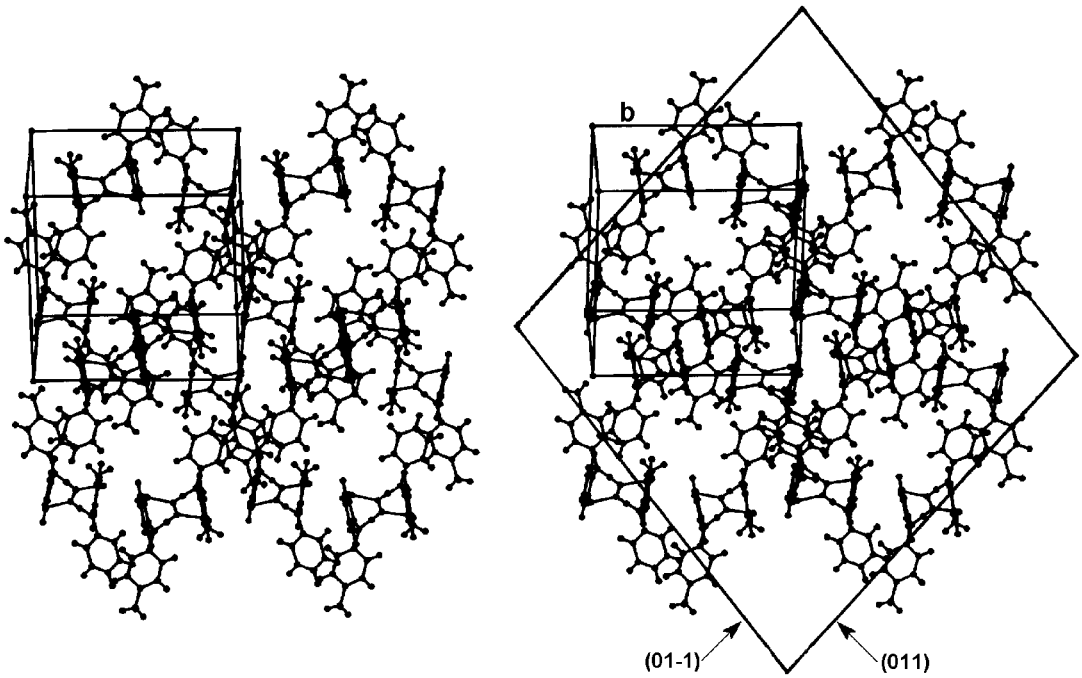

Figure 5. Stereoscopic image of the crystal packing of *rac*-**1** on the (–101) face showing favorable alignment in the vertical diagonal between the edges of the natural (011) and (01–1) faces that are indicated in the right part of the image

apparently used for the long-range molecular migrations. The DSC results (*meso*-**1**, exotherm at 178 °C, melt at 216 °C; *rac*-**1**, exotherm at 150 °C, melt at 193 °C)[4] and the enormous vertical and lateral resolution of AFM exclude submicromelting[1,8,9] during reaction as the very sharp features in Figs 1(b) and 2(b) and (c) developed gradually at several interrupted heating periods. We do not precisely match the same spot in the discontinuous technique and keep away from surface defects and cracks. However, numerous measurements in the region of the typical initial site secure uniformity of the features, which is more important for the validity of the conclusions.

The final crystals of **3** and **5** + **6** (as obtained) are not single crystals. They are turbid, have microscopic cracks and are no longer suitable for x-ray diffraction with a diffractometer.

The geometric changes and the space demand are extraordinarily high in both of our systems (Scheme 1). It might therefore be expected that the reaction rate is higher in the surface region than in the bulk. Nevertheless, we do have high overall conversions and finally complete reaction.[4,5] The large [Fig. 1(d)] and very large features [Fig. 2(d)] that form and the cracks at high conversions are clear evidence of non-topotactic bulk reactions. The crystals keep their macroscopic shape[4,5] but they are not converted into single crystals, as is shown by the submicro- and micro-features in the AFM images of Figs 1 and 2. There are thus major differences from the behavior of *rac*-3,8-di-*tert*-butyl-1,5,6,10-tetraphenyl-deca-(3,4,6,7)-tetraene-(1,9)-diyne in Ref. 3 that gave thermal unimolecular reaction only at outer and inner surfaces.

EXPERIMENTAL

Single crystals of *meso*-**1** and *rac*-**1** were obtained by slow evaporation of solutions in ethyl acetate. Flat laths of *meso*-**1** ($1.2 \times 0.3 \times 0.05\,mm^3$) and plates of *rac*-**1** ($1.0 \times 1.0 \times 0.2\,mm^3$) were selected and the Miller indices determined on an x-ray diffractometer.

AFM techniques (Nanosope II) and 3D-data analyses have been described elsewhere in much detail.[1] Only non-scraping pyramidal cantilever tips of Si_3N_4[1,8,10] were used throughout. The crystals were glued to a magnetic support on a conducting tab. After AFM measurements of the untreated crystal in a uniform region, the sample was inserted in a flat vessel, evacuated and heated at 130 °C in an oven for the specified times. After remounting, several AFM measurements were performed as close as possible to the initial site where a change in angle of measurement with respect to the crystal edges might have been necessary for an optimized image. In parallel runs, good quality crystals with similar sizes of *meso*-**1** or *rac*-**1** were placed as single layers in the flat vessel and heated under vacuum at 130 °C for 15 or 15 and 30 min in the same environment for ^1H NMR analysis.

A Perkin-Elmer Lambda 15 UV/VIS spectrometer was used for absorption spectra and Beer's law secured by

dilution to half and one quarter of the initial concentration. Microscopic inspections were performed on a Zeiss microscope. Published x-ray data were used.[4] The packing diagrams were obtained using SCHAKAL 97 software of E. Keller, University of Freiburg.

Supplementary material

The supplementary material available at the epoc website at http://www.wiley.com/epoc contains the color images in GIF format and interactively usable full original 3D data of the images in VRML format in high and low resolution in order to allow for critical evaluation of the AFM results, their analytical use with suitable imaging software and future data mining. Interactive viewing is possible with public domain software, e.g. Cosmo Player or Blaxxun, via Internet Explorer.

REFERENCES

1. Kaupp G. In *Comprehensive Supramolecular Chemistry*, vol. 8, Davies JED (ed). Elsevier: Oxford, 1996; 381–423 + 21 color plates.
2. Kaupp G, Schmeyers J. *J. Photochem. Photobiol. B* 2000; **59**: 15–19.
3. Kaupp G, Schmeyers J, Kato M, Tanaka K, Harada N, Toda F. *J Phys. Org. Chem.* 2001; **14**: 444–452.
4. Toda F, Tanaka K, Tamashima T, Kato M. *Angew. Chem., Int. Ed. Engl.* 1998; **37**: 2724–2727.
5. Toda F. *Eur. J. Org. Chem.* 2000; 1377–1386.
6. Nakanishi H, Jones W, Thomas JM, Hursthouse MB, Motevalli M. *J. Phys. Chem.* 1981; **85**: 3636–3642.
7. Kohlschütter V. *Z. Anorg. Allg. Chem.* 1919; **105**: 1–25.
8. Kaupp G. *J. Vac. Sci. Technol. B* 1994; **12**: 1952–1956.
9. Kaupp G. *Mol. Cryst. Liq. Cryst.* 1992; **211**: 1–15; Kaupp G. *Mol. Cryst. Liq. Cryst.* 1994; **242**: 153–169.
10. Kaupp G, Plagmann M. *J. Photochem. Photobiol. A* 1994; **80**: 399–407; Kaupp G, Schmeyers J, Pogodda U, Haak M, Marquardt T, Plagmann M. *Thin Solid Films* 1995; **264**: 205–211.